AJNR

Biometry of the Cerebellar Vermis and Brain Stem in Children: MR Imaging Reference Data from Measurements in 718 Children

C. Jandeaux, G. Kuchcinski, C. Ternynck, A. Riquet, X. Leclerc, J.-P. Pruvo and G. Soto-Ares

This information is current as of June 18, 2025.

Biometry of the Cerebellar Vermis and Brain Stem in Children: MR Imaging Reference Data from Measurements in 718 Children

C. Jandeaux, G. Kuchcinski, C. Ternynck, A. Riquet, X. Leclerc, J.-P. Pruvo, and G. Soto-Ares

ABSTRACT

BACKGROUND AND PURPOSE: Objective and quantitative data to define cerebellar vermis and/or brain stem hypoplasia in children are lacking. Our aim was to provide MR imaging biometric references for the cerebellar vermis and brain stem from a large cohort of children with normal cerebellums.

MATERIALS AND METHODS: The MR imaging data were retrospectively selected from our hospital data base from January 1, 2014, to December 31, 2017. All MR imaging examinations of children between 1 day and 15 years of age, including midline sagittal sections, were included. Children with a clinical history or MR imaging abnormalities that may affect the posterior fossa were excluded. We manually measured four 2D parameters: vermian height, anterior-posterior diameter of the vermis, anterior-posterior diameter of the midbrain-pons junction, and anterior-posterior midpons diameter. The inter- and intraobserver agreement was evaluated.

RESULTS: Seven hundred eighteen children were included (372 boys and 346 girls), from 1 day to 15 years of age. Normal values (third to 97th percentiles) were provided for each parameter. The vermis parameters showed a rapid growth phase during the first year, a slower growth until the fifth year, and finally a near-plateau phase. The brain stem parameters showed more progressive growth. The intra- and interobserver agreement was excellent for all parameters.

CONCLUSIONS: We provide reference biometric data of the vermis and the brain stem using simple and reproducible measurements that are easy to use in daily practice. The relevance of these 2D measurements should be further validated in diseases associated with cerebellar abnormalities.

ABBREVIATIONS: APD-MP = anterior-posterior diameter at the midbrain-pons junction; APD-P = anterior-posterior midpons diameter; APD-V = anterior-posterior diameter of vermis; H-V = vermian height; ICC = intraclass correlation coefficient

The important role of the cerebellum in nonmotor functions has been confirmed in recent studies performed in healthy subjects.[1,2] In this setting, the diagnosis of cerebellar hypoplasia is essential, particularly in children with mental retardation in whom impairment in cerebellar cognitive functions is frequently observed.[3] Cerebellar hypoplasia has been further associated with impairment in reasoning, spatial recognition, language, timing of the speech, and disorders of personality.[4-6]

Even if different methods of volumetry and segmentation have already been reported in the literature,[7-9] the interpretation of the vermis as normal or pathologic in daily routine is only based on subjective criteria. Because morphologic variations and changes occur throughout infancy, this subjective approach may be inappropriate to state the normality of the vermis or to claim the diagnosis of vermian hypoplasia, which is defined as a small, harmonious vermis with fissures of normal width.[10] Pons hypoplasia has been also described in association with vermis abnormalities in specific syndromes such as pontocerebellar hypoplasia.[11]

To our knowledge, no reference data have been published that can be easily used in daily practice to define vermis or pons hypoplasia. The aim of our study was to provide reference biometric data of the vermis and brain stem from a large cohort of children with normal cerebellums and brain stems to increase the accuracy of MR imaging for the diagnosis of vermis and/or pons hypoplasia.
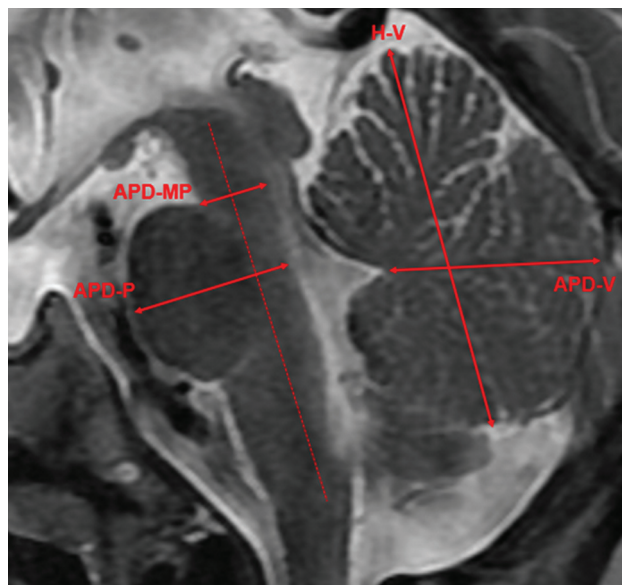
FIG 1. Illustration of the 2D measurements of the cerebellar vermis and the brain stem. H-V indicates the largest craniocaudal diameter of the vermis; APD-V, the largest anterior-posterior diameter of the vermis passing through the tip of the V4; APD-MP, perpendicular to the major axis of the brain stem passing through the midbrain-pons junction; APD-P, perpendicular to the major axis of the brain stem passing through the middle of the pons.

Table 1: Distribution of the study population by age and sex (n = 718)

Age Class (yr)	Boys (n = 372)	Girls (n = 346)	All (n = 718)
Younger than 1	58	56	114
1–2	37	32	69
2–3	39	28	67
3–4	31	22	53
4–5	27	23	50
5–6	20	21	41
6–7	30	18	48
7–8	17	17	34
8–9	9	16	25
9–10	16	12	28
10–11	10	12	22
11–12	11	14	25
12–13	11	18	29
13–14	13	20	33
14–15	17	19	36
15–16	26	18	44

MATERIALS AND METHODS

Population

The protocol has been approved by our institutional review board. Given the retrospective nature of the study, informed consent from the parents was not required. The MR imaging data were nonconsecutive cases selected retrospectively from our hospital data base from January 1, 2014, to December 31, 2017.

MR imaging examinations of children between 1 day and 15 years of age, including midline sagittal sections from 2D or 3D T1- or T2-weighted sequences, were included. All children in the present study had no self- or parent-reported clinical history of cognitive disorders or mental illness that could have a potential impact on the cognitive status and cerebellum alteration. We also excluded all patients with a history or symptoms that may be responsible for or associated with cerebellar abnormalities: prematurity (birth at <37 weeks of amenorrhea according to the World Health Organization), metabolic disorder, neuropsychological disorder, hypoxic pathology, cerebellar syndrome, autistic syndrome, axial hypotonia, delayed acquisition, posterior fossa pathology, and posterior fossa or midline malformation. All MR images were reviewed by a board-certified pediatric neuroradiologist to ensure that there were no posterior fossa abnormalities. Mass effect, signal abnormalities, vermian or pons hypoplasia, atrophy, and other midline malformations were sought, and if present, the corresponding data were excluded. The MR imaging data that did not allow precise measurements because of unsatisfactory quality were also excluded.

MR Imaging Analysis

All acquisitions were performed on a 1.5T MR imaging scanner (Ingenia; Philips Healthcare, Best, the Netherlands). Midline sagittal sections were obtained from 2D sagittal T1- or T2-weighted sequences or reconstructed from 3D T1-weighted sequences (section thickness, ≤3 mm).

All measurements were performed by a board-certified neuroradiologist. Simple 2D measurements were manually performed on a sagittal section passing through the midsagittal plane and were defined as follows: 1) The height of the vermis (H-V) was the largest craniocaudal diameter of the vermis; 2) the anterior-posterior diameter of the vermis (APD-V) was the largest anterior-posterior diameter of the vermis passing through the tip of the V4; 3) the anterior-posterior diameter of the midbrain-pons junction (APD-MP) was measured perpendicular to the major axis of the brain stem passing through the midbrain-pons junction; and 4) the anterior-posterior midpons diameter (APD-P) was measured perpendicular to the major axis of the brain stem passing through the middle of the pons (Fig 1).

To evaluate the interobserver reproducibility, a second senior neuroradiologist performed the measurements independently on a sample of 50 children randomly selected. Each radiologist was unaware of the results obtained by the other one. Moreover, to evaluate the intraobserver reproducibility, the first reader repeated the measurements on the same sample after 1 month.

Statistical Analysis

We first assessed the intra- and interobserver reproducibility of measurements of the cerebellar vermis by calculating the intraclass correlation coefficient (ICC) and using the Bland-Altman method on a random sample of 50 patients. The ICCs were estimated using a 2-way random-effects model (absolute agreement), and 95% confidence intervals were obtained using bootstrap methods (2000 bootstrap samples). ICC values <0.5, between 0.5 and 0.75, between 0.75 and 0.9, and >0.90 were interpreted as poor, moderate, good, and excellent reproducibility.[12] According to the Bland Altman method,[13] we calculated the mean bias as well as the limits of agreement between readers. The remaining data analyses were performed on the overall study sample to provide age-specific reference intervals ("normal ranges") for each

Table 2: Indications for brain MR imaging in the study population (*n* = 718)

Diseases	Prevalence
Epilepsy	123 (17.2%)
Supratentorial, suprasellar, or optic tumors	65 (9%)
Ocular globe pathology	56 (7.7%)
Suspicion of pituitary lesion (staturo-pondéral growth retardation, obesity, and so forth)	55 (7.6%)
Encephalitis, mastoiditis, meningitis, endocarditis, otitis, or empyema	52 (7.3%)
Extracerebral tumor or histiocytosis or blood disease	40 (5.6%)
Cranial trauma	37 (5.2%)
Spinal or medullary pathology, scoliosis, low back pain	36 (5%)
Supratentorial benign lesion (arachnoid cyst, pineal cyst, interhemispheric cyst, and so forth)	32 (4.4%)
Extracerebral or supratentorial vascular malformation	28 (3.9%)
Extracerebral venous-lymphatic malformation	26 (3.6%)
Isolated cervicofacial pathology (cervical mass, velar insufficiency, and so forth)	21 (2.9%)
Cyst or nasal root mass	19 (2.6%)
Headache	15 (2.1%)
Deafness	10 (1.4%)
Others	103 (14.5%)

Table 3: Equation for estimating reference values for the different parameters[a]

	Equations
H-V girls	$\mu = 443\,574.11 - 97\,540.24\sqrt{X} - 231\,497.89X^3$ $\sigma = 104\,925.72 - 37\,776.52X$
H-V boys	$\mu = 707\,969.47 - 45\,502.94\log X - 538\,257.55X^3$ $\sigma = 200\,387.18 - 82\,416.42X$
APD-V girls	$\mu = 585.75 - 336.12X^3$ $\sigma = 121.27$
APD-V boys	$\mu = 1\,083.91 - 689.41X^3$ $\sigma = 226.61$
APD-P girls	$\mu = 38.13 - 2\log X - 10.21X^3$ $\sigma = 4.09$
APD-P boys	$\mu = 83.63 - 6.40\log X - 31.23X^3$ $\sigma = 12.09 - 4.71X$
APD-MP	$\mu = 5.98 + 0.053X^{-0.05} - 1.31X$ $\sigma = 0.48$

[a] With $X = \exp\left\{\frac{T-T_1}{T_n-T_1}\log\rho\right\}$, where T denotes the age, T_1 and T_n denote minimum and maximum ages, respectively, and ρ is a preselected constant for which a suitable value is .01. All measurements needed prior Box-Cox transformation. The values of APD-MP were similar in both sexes.

measurement of the cerebellar vermis. To appreciate the shape of the relationship between age and each measurement of interest and to investigate the necessity to provide age-specific reference intervals by sex, we used a nonparametric smoothing technique (LOESS regression). Age-specific reference intervals for each measurement of interest were constructed from the parametric method proposed by Royston and Wright,[14] providing smooth centile curves and explicit formulae for the centile estimates. This method has been previously applied to provide reference biometric data of the corpus callosum in MR imaging in children[15] and is one of the methods recommended by the World Health Organization Multicenter Growth Reference Study Group. Further details about this method are available in the On-line

Appendix. All analyses were computed using R statistical and computing software, Version 3.4.3 (http://www.r-project.org/).

RESULTS

We included 718 children (372 boys and 346 girls), from 6 days to 15 years of age. The distribution of the number of children as a function of age and sex is described in Table 1. Table 2 shows the indications of MR imaging for the children included in the study. Measurements were performed on T2 images in 331 children and on T1 images in 387. The average time to complete the 4 measurements was 1 minute.

The 7 models built were normal, and the 7 measurements needed prior Box-Cox transformation. The equations for estimating the reference values for the different parameters are presented in Table 3. Smoothing curves of the different parameters are depicted in Fig 2. For each parameter, reference values (from the third, median, and 97th percentiles) are depicted in Fig 3 and summarized in On-line Table 1. Model adequacy was satisfied for all models (On-line Figs 1 and 2). The curves showed similar growth in girls and boys. Vermis parameters (H-V, APD-V) showed a very rapid growth phase during the first year, then a slower growth until the fourth year, and finally a near-plateau phase. Brain stem parameters showed a different growth pattern, more progressive, with relatively rapid growth during the first 4 years and then slower thereafter. The values of these parameters were higher in boys except for APD-MP, which demonstrated similar values in both sexes. As shown in Table 4, the intraobserver agreement was excellent for each parameter, with an ICC ranging from 0.916 to 0. 994. The interobserver agreement was good to excellent, with an ICC ranging from 0.846 for APD-P to 0.981 for H-V. Intra- and interobserver agreement did not significantly differ for measurements performed on T1 or T2 images (On-line Table 2).

DISCUSSION

Our study used a simple method, easily reproducible in daily practice in a large cohort of children with normal vermes and brain stems. Findings showed an important growth of the vermian parameters during the first year, while the brain stem
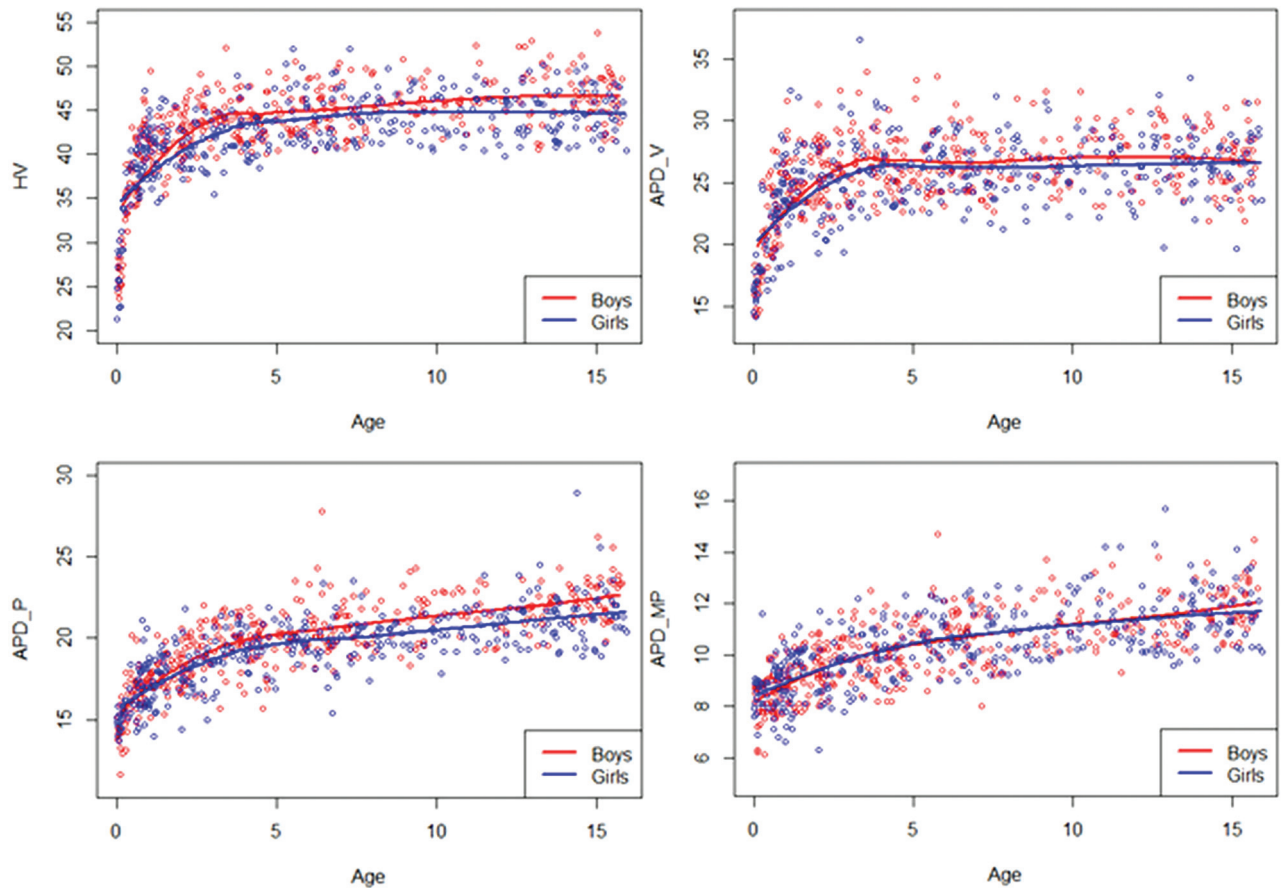
FIG 2. Smoothed curves of the different parameters (H-V, APD-V, APD-P, APD-MP) by age and sex.

parameters grew gradually. The values of these parameters were higher in boys except for APD-MP, for which the values were similar in both sexes.

To our knowledge, this is the first reference biometric data for the vermis and the brain stem in children. Previous studies assessed normal MR imaging biometric data of the posterior fossa in the fetus,[7,16-18] and quantitative methods have already been used to diagnose vermis hypoplasia, but no MR imaging biometric data of the normal cerebellum and brain stem have been reported before. Makris et al[9] described a surface-based parcellation of the human cerebellar cortex and provide cerebellar surface and volumetry from 10 volunteer subjects with a good-to-excellent reproducibility. This method integrated automated and semiautomated and manual procedures using postprocessing software. Joyal et al[19] suggested measuring the area of the vermis from a single midsagittal section, but reproducibility has not been studed. In addition, both studies were performed in the adult population, and their methodology is not easy to apply in daily practice. Our 2D measurements have the advantage of being highly reproducible, easy, and fast to perform. An interactive tool derived from the biometric models has been created and is available on-line (http://ci2c.fr/vermis.php) to facilitate its application.

Data about the growth of the cerebellum during childhood are scarce. During fetal life, the cerebellum has a long period of development that makes it particularly vulnerable to prenatal

disorders, including genetic or metabolic diseases, toxins, or infections.[20-22] In early stages, perturbations of the expression of genes involved in cerebellar patterning or abnormal proliferation and migration produce a wide spectrum of abnormal phenotypes from agenesis to minor abnormalities such as hypoplasia or abnormal cerebellar foliation. The fastest development is observed for the vermis and the cerebellum in comparison with other brain structures in the third trimester of pregnancy.[17] Their growth is multiplied by 2 between the 20th and the 35th week of development.[23] As the proliferation and migration of granular cells continue during the first postnatal months, the last granular cell migration occurs in humans at about 18 months of age. In line with previous studies suggesting further proliferation and neuronal migration in the cerebellum during the postnatal period,[20,24,25] our data show the persistence of a rapid growth of the vermis during the first year of life.

Cerebellar hypoplasia has been described in many conditions associated with mental retardation.[3-5,26] In this setting, morphologic variations may disclose underlying structural and functional impairment of cerebellar structures potentially involved in cognitive functions. Advanced MR imaging techniques such as DTI-based tractography have emphasized the anatomic relationship between the cerebellum and the other structures of the central nervous system involved in nonmotor functions,[27] especially dentato-thalamo-cortical fibers and fibers connecting the cerebellum to visuospatial, cognitive, and memory-related areas, in healthy
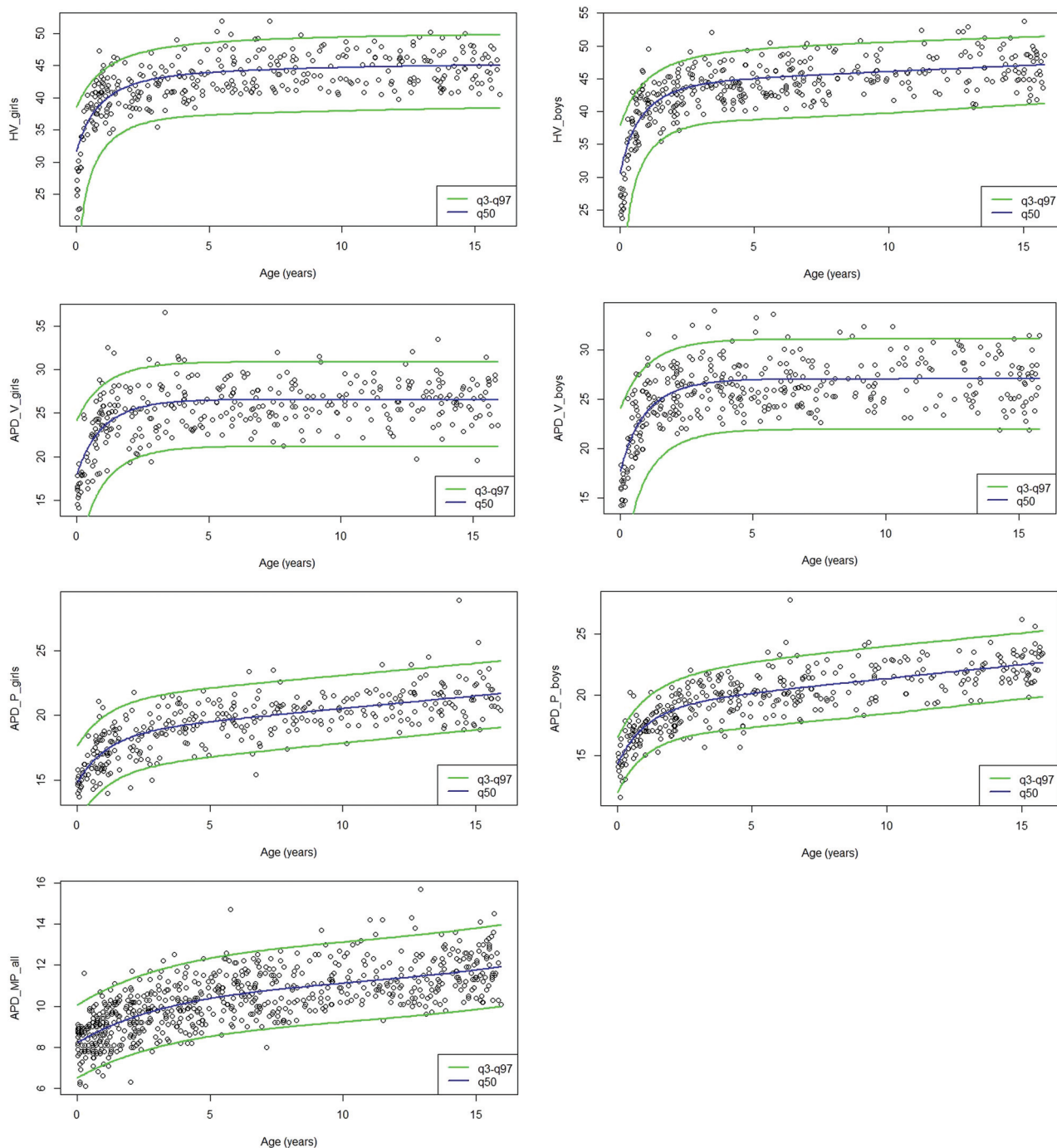
FIG 3. Reference intervals (third, 50th, 97th) for the different parameters (H-V, APD-V, APD-P, APD-MP). The values of APD-MP are similar in both sexes.

Table 4: Inter- and intraobserver agreement for cerebellar vermis and brain stem parameters

Parameter	Intraobserver Agreement			Interobserver Agreement		
	Mean Bias	95% Limits of Agreement	ICC (95% CI)	Mean Bias	95% Limits of Agreement	ICC (95% CI)
H-V	0.156	0.869, 1.181	0.994 (0.982–0.998)	−0.302	−2.129, 1.525	0.981 (0.948–0.991)
APD-V	0.332	1.831, 2.494	0.941 (0.878–0.970)	0.242	−2.851, 3.335	0.893 (0.799–0.948)
APD-P	0.100	−1.161, 1.361	0.916 (0.854–0.953)	0.088	1.704, 1.880	0.846 (0.674–0.944)
APD-MP	0.052	−0.729, 0.833	0.988 (0.978–0.994)	0.188	−1.238, 1.614	0.959 (0.918–0.978)

subjects.[27-29] Furthermore, in children with cerebellar hypoplasia, impairment of cerebellar white matter tracts has been observed in preliminary studies.[30] These structural data have been strengthened by functional MR imaging studies exploring the anatomofunctional segmentation of the cerebellum.[1] These studies highlighted a limbic area corresponding to lobules VI and VII,[31] left lateralization of the activation on visuospatial tasks, right activation in linguistic and working memory tasks,[2] and activation of the anterior lobes in language articulation, whereas the posterior lobules were activated in silent langage.[32]

Our study has some limitations. First, our study population consisted of nonconsecutive cases examined retrospectively. We acknowledge that while effort was made to exclude children with posterior fossa abnormalities, we included children with pathologies that could potentially affect the cerebellum despite a macroscopically normal appearance on MR imaging. For children older than 6 years of age, our results should be confirmed by larger trials imaging strictly healthy children. Although measurements have been performed on different MR images, this feature did not significantly affect their reliability. Finally, our global measurements do not allow detecting a focal cerebellar hypoplasia involving a single lobe or lobule. Further studies are necessary to confirm the accuracy of our biometric data when applied to the evaluation of children with vermian hypoplasia and other posterior fossa abnormalities.

CONCLUSIONS

We provide reference biometric data of the vermis and the brain stem using simple and reproducible measurements that are easy to use in daily practice. Our results show a more important growth of the vermian parameters during the first year of life, while the brain stem parameters grow gradually. The relevance of these 2D measurements should be further validated in diseases associated with cerebellar abnormalities responsible for developmental disorders of so-called higher cerebellar functions.

REFERENCES

1. Klein AP, Ulmer JL, Quinet SA, et al. **Nonmotor functions of the cerebellum: an introduction.** *AJNR Am J Neuroradiol* 2016;37:1005–09 CrossRef Medline
2. Timmann D, Drepper J, Frings M, et al. **The human cerebellum contributes to motor, emotional and cognitive associative learning: a review.** *Cortex* 2010;46:845–57 CrossRef Medline
3. Soto-Ares G, Joyes B, Lemaître MP, et al. **MRI in children with mental retardation.** *Pediatr Radiol* 2003;33:334–45 CrossRef Medline
4. Schmahmann JD, Sherman JC. **The cerebellar cognitive affective syndrome.** *Brain* 1998;121:561–79 CrossRef Medline
5. Cotes C, Bonfante E, Lazor J, et al. **Congenital basis of posterior fossa anomalies.** *Neuroradiol J* 2015;28:238–53 CrossRef Medline
6. Shevell MI, Majnemer A. **Clinical features of developmental disability associated with cerebellar hypoplasia.** *Pediatr Neurol* 1996; 15:224–29 CrossRef Medline
7. Kyriakopoulou V, Vatansever D, Davidson A, et al. **Normative biometry of the fetal brain using magnetic resonance imaging.** *Brain Struct Funct* 2017;222:2295–307 CrossRef Medline
8. Ber R, Hoffman D, Hoffman C, et al. **Volume of structures in the fetal brain measured with a new semiautomated method.** *AJNR Am J Neuroradiol* 2017;38:2193–98 CrossRef Medline
9. Makris N, Schlerf JE, Hodge SM, et al. **MRI-based surface-assisted parcellation of human cerebellar cortex: an anatomically specified method with estimate of reliability.** *Neuroimage* 2005;25:1146–60 CrossRef Medline
10. Adamsbaum C, Merzoug V, André C, et al. **Imaging of the pediatric cerebellum [in French].** *J Neuroradiol* 2003;30:158–71 Medline
11. Namavar Y, Barth PG, Poll-The BT, et al. **Classification, diagnosis and potential mechanisms in pontocerebellar hypoplasia.** *Orphanet J Rare Dis* 2011;6:50 CrossRef Medline
12. Koo TK, Li MY. **A guideline of selecting and reporting intraclass correlation coefficients for reliability research.** *J Chiropr Med* 2016;15:155–63 CrossRef Medline
13. Bland JM, Altman DG. **Statistical methods for assessing agreement between two methods of clinical measurement.** *Lancet* 1986;1:307–10 Medline
14. Royston P, Wright E. **A method for estimating age-specific reference intervals ('normal ranges') based on fractional polynomials and exponential transformation.** *Journal of the Royal Statistical Society Series A (Statistics in Society)* 2002;161:79–101 CrossRef
15. Garel C, Cont I, Alberti C, et al. **Biometry of the corpus callosum in children: MR imaging reference data.** *AJNR Am J Neuroradiol* 2011;32:1436–43 CrossRef Medline
16. Saleem SN. **Fetal magnetic resonance imaging (MRI): a tool for a better understanding of normal and abnormal brain development.** *J Child Neurol* 2013;28:890–908 CrossRef Medline
17. Chang CH, Chang FM, Yu CH, et al. **Assessment of fetal cerebellar volume using three-dimensional ultrasound.** *Ultrasound Med Biol* 2000;26:981–88 CrossRef Medline
18. Ber R, Bar-Yosef O, Hoffmann C, et al. **Normal fetal posterior fossa in MR imaging: new biometric data and possible clinical significance.** *AJNR Am J Neuroradiol* 2015;36:795–802 CrossRef Medline
19. Joyal CC, Pennanen C, Tiihonen E, et al. **MRI volumetry of the vermis and the cerebellar hemispheres in men with schizophrenia.** *Psychiatry Res* 2004;131:115–24 CrossRef Medline
20. Ten Donkelaar HJ, Lammens M. **Development of the human cerebellum and its disorders.** *Clin Perinatol* 2009;36:513–30 CrossRef Medline
21. Basson MA, Wingate RJ. **Congenital hypoplasia of the cerebellum: developmental causes and behavioral consequences.** *Front Neuroanat* 2013;7:29 CrossRef Medline
22. Bosemani T, Poretti A. **Cerebellar disruptions and neurodevelopmental disabilities.** *Semin Fetal Neonatal Med* 2016;21:339–48 CrossRef Medline
23. Cignini P, Giorlandino M, Brutti P, et al. **Reference charts for fetal cerebellar vermis height: a prospective cross-sectional study of 10605 fetuses.** *PLoS One* 2016;11:e0147528 CrossRef Medline
24. Garel C, Fallet-Bianco C, Guibaud L. **The fetal cerebellum: development and common malformations.** *J Child Neurol* 2011;26:1483–92 CrossRef Medline
25. Chédotal A. **Should I stay or should I go? Becoming a granule cell.** *Trends Neurosci* 2010;33:163–72 CrossRef Medline
26. Berthel-Tatray MC. **Le syndrome cognitivo-affectif du cervelet.** *Rev Neurol (Paris)* 2017;173:S184 CrossRef
27. Granziera C, Schmahmann JD, Hadjikhani N, et al. **Diffusion spectrum imaging shows the structural basis of functional cerebellar circuits in the human cerebellum in vivo.** *PLoS One* 2009;4:e510v CrossRef Medline
28. Habas C, Cabanis EA. **Cortical projection to the human red nucleus: complementary results with probabilistic tractography at 3 T.** *Neuroradiology* 2007;49:777–84 CrossRef Medline

29. Jissendi P, Baudry S, Balériaux D. **Diffusion tensor imaging (DTI) and tractography of the cerebellar projections to prefrontal and posterior parietal cortices: a study at 3T.** *J Neuroradiol* 2008;35:42–50 CrossRef Medline

30. Fiori S, Poretti A, Pannek K, et al. **Diffusion tractography biomarkers of pediatric cerebellar hypoplasia/atrophy: preliminary results using constrained spherical deconvolution.** *AJNR Am J Neuroradiol* 2016;37:917–23 CrossRef Medline

31. Baumann O, Mattingley JB. **Functional topography of primary emotion processing in the human cerebellum.** *Neuroimage* 2012; 61:805–11 CrossRef Medline

32. Méndez Orellana C, Visch-Brink E, Vernooij M, et al. **Crossed cerebrocerebellar language lateralization: an additional diagnostic feature for assessing atypical language representation in presurgical functional MR imaging.** *AJNR Am J Neuroradiol* 2015;36:518–24 CrossRef Medline